

## FLOW CONTROL ON HELICOPTER-ROTOR BLADES VIA ACTIVE GURNEY FLAP<sup>1</sup>

**Wienćzysław Stalewski**

Institute of Aviation

al. Krakowska 110/114, 02-256 Warsaw, Poland

*Wienćzyslaw.Stalewski@ilot.edu.pl*

### **Abstract**

The Active Gurney Flap (AGF) is a small, flat tab cyclically deployed and retracted at lower surface of the rotor blade near its trailing edge. It is expected that the device may improve performance of modern helicopters. The main goal of presented investigations was to develop research methodology and next to use it in studies on phenomena occurring in the flow around helicopter-rotor blades equipped with AGF. Conducted CFD simulations aimed at validation of the developed methodology as well as at significant supplementing and extension of results of experimental research. Simplified sensitivity analysis has been conducted aiming at determination of geometric and motion-control parameters of the AGF, optimal from point of view of helicopter-performance improvement. Fully three-dimensional simulations of the rotor flight aimed at determination of flight conditions, in which the use of Active Gurney Flaps could significantly improve the rotorcraft performance.

**Keywords:** helicopter rotor blades, active flow control, Active Gurney Flap, rotorcraft performance.

## **1. INTRODUCTION**

Active flow control on helicopter-rotor blades is one of very promising directions of development in Rotorcraft Engineering, aiming at improvement both the performance and environmental impact of modern helicopters.

Flow on rotor blades may be controlled by different means, including: fluidic devices [1], vortex generators [2] or mechanical devices mounted in proximity of blade trailing edge [3]. The solution presented in this paper belongs to the third of above groups and is named Active Gurney Flap (AGF).

---

<sup>1</sup> This is an extended version of the paper presented at 30<sup>th</sup> Congress of International Council of the Aeronautical Sciences (ICAS), Daejeon, Korea, September 25<sup>th</sup> - 30<sup>th</sup>, 2016.

The classic Gurney Flap [4] is a small, flat tab located at a pressure side of lifting surface near its trailing edge. The tab deflects the air stream behind the trailing edge downwards, leading to lift increase. In helicopter applications, instead of static tab, the dynamically deployed and retracted Gurney flap is more useful, because of strong dynamic effects in flow during rotorcraft flight.

In Rotorcraft Engineering, the Active Gurney Flap is a small, flat tab located at lower surface of the blade near its trailing edge. The tab is cyclically deployed and retracted perpendicularly to the blade surface. When deployed, the tab deflects air stream behind the trailing edge downwards, leading to lift increase, which is especially important on the retreating blade of the rotor. On the advancing blade, the AGF is retracted to minimise rotor torque. Such performance-enhancement application of the AGF is realised in one deployment-retreatment cycle per one revolution of the rotor. Higher frequencies of AGF motion are considered for vibration-control purposes. Due to technical limitations, the deployable tab is usually located at certain distance from the trailing edge of the blade, as shown in Figure 1. The AGF-type device, through active control of the flow on the blades may significantly improve aerodynamic properties of the rotor. However, to take full advantage of potential benefits of AGF applications it is necessary to gain knowledge about physical phenomena that occur in the flow around such configurations. Eventually, the knowledge should help to answer the question: how to design, implement and control the AGF-type devices so as to gain maximum profits, e.g. significant improvement of helicopter performance.

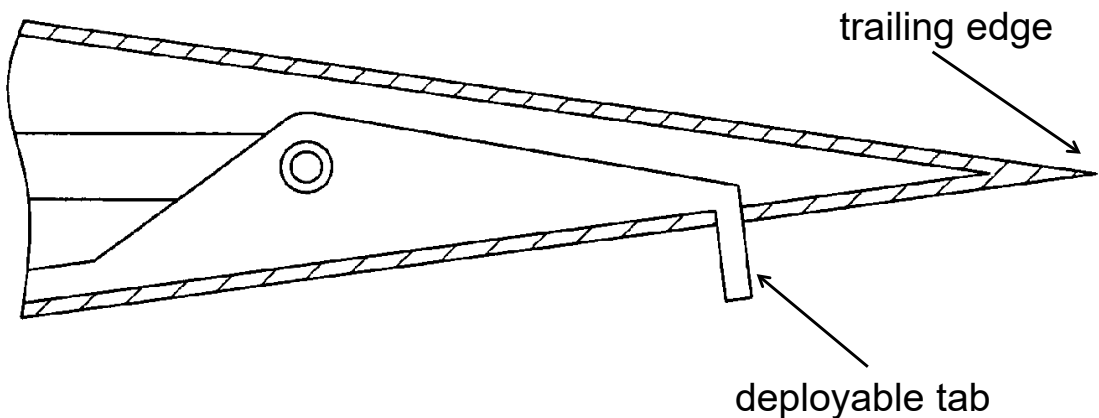


Fig. 1. Scheme of implementation of the AGF on helicopter blade taken from the Patent of Active Gurney Flap [5]

## 2. METHODOLOGY

The general scheme of developed methodology of simulation of forward flight of helicopter main rotor is shown in Figure 2. In the presented approach, the simulation of rotor flight consists in the solution of unsteady Navier-Stokes Equations in time-varying domain surrounding the rotating rotor. The Navier-Stokes Equations are solved using the commercial code ANSYS FLUENT [6]. All computational

activities concerning specific rotorcraft aspects, including the AGF motion, are performed by the developed code Virtual-Rotor-3D which is compiled module of User Defined Functions, linked with essential code of ANSYS FLUENT. Among others, the module Virtual-Rotor-3D is responsible for modelling of:

- rotor forward flight and rotational motion
- feathering of the rotor blade, resulting from assumed collective and cyclic pitch controls and pitch-flap coupling
- flap and lag motion of the blades around flap and lag hinges
- cyclic motion of the AGF

Coupled equations of flap and lag motion of the blades are solved simultaneously with the solution of Navier-Stokes Equations, taking into account effects of dampers and springs, if any. The flap-and-lag motion is described by the system of four ordinary differential equations of the first order on four unknown functions:  $\beta(t)$ ,  $\zeta(t)$ ,  $\beta'(t)$ ,  $\zeta'(t)$  where  $\beta$  is the flap angle,  $\zeta$  is the lag angle,  $\beta' = d\beta/dt$ ,  $\zeta' = d\zeta/dt$ .

The blade pitch controls may be changed during the simulation which is used when trimming the rotor so as to obtain required thrust and moments. Alternative trimming procedure, so called “zero-flapping” consists in establishing the cyclic pitch controls so as to obtain zero 1<sup>st</sup>-harmonics of blade flapping. The input data consist of computational mesh and three data sets describing: flight conditions, flight controls and rotor data.

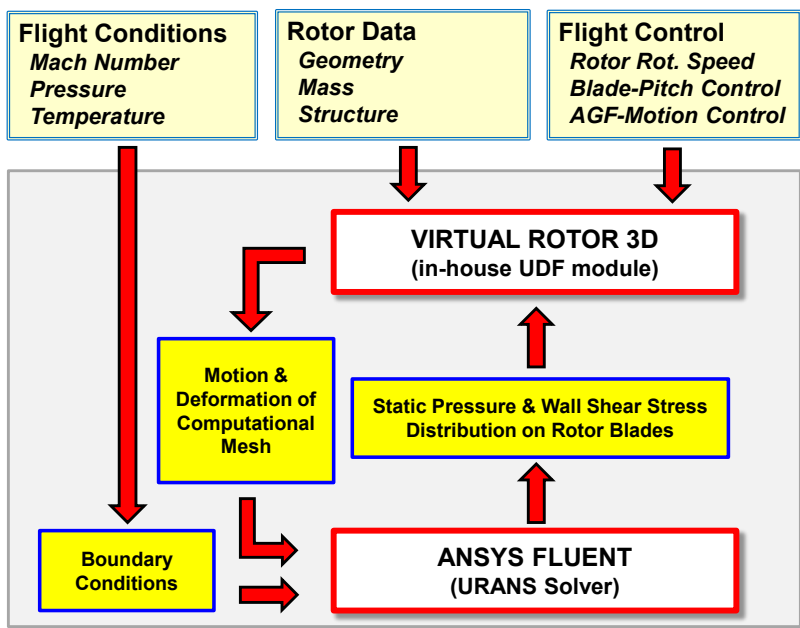


Fig. 2. The general scheme of developed methodology of simulation of flight of helicopter main rotor with blades equipped with AGF

In presented approach, the computational mesh is divided into several subdomains. Overall topological structure of the mesh is presented in Figure 3. Around each blade, the cylinder-conical volume zone is defined. Such zones are embedded in a cylinder-volume zone which is embedded in a far-field, cuboid zone.

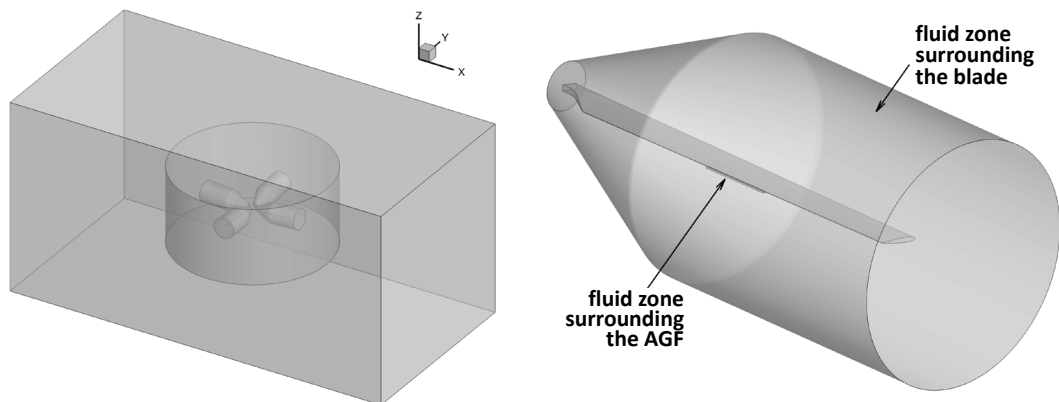


Fig. 3. Overall topology of computational mesh

During the rotor flight simulation, the mesh surrounding each blade is moving together with the blade. This motion is a combination of feathering, flapping and lead-lag motion. Additionally the mesh surrounding each blade is rotating together with the cylindrical zone, around the rotor-rotation axis. The motion of meshes surrounding the blades, relative to the cylindrical zone, is realised by the use of Dynamic Mesh and Sliding Mesh techniques implemented in the ANSYS FLUENT solver. The rotational motion of the cylindrical zone inside the far-field zone is also realised based on the Sliding Mesh technique.

During the rotor flight simulation, the mesh surrounding each blade is locally deformed so as to model a movement of the AGF. Sequential stages of such deformation are presented in Figure 4. During gradual deflection of the AGF, the mesh is gradually stretched on it. During retraction of the AGF, similar deformation is performed in inverse direction. Presented method of simulation of the AGF movement was developed specially for purposes of COMROTAG project. The method ensures high quality of the deformed mesh (including preserving high-quality of boundary-layer mesh of  $Y^+ \sim 1$ ) as well as full repeatability of deformations. Presented approach is an alternative to the Overlapping Grid Methods [7], usually utilised in such cases.

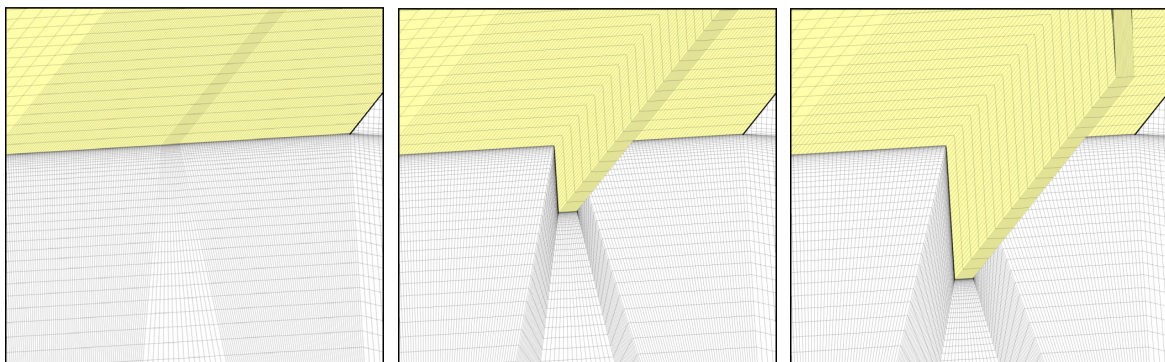


Fig. 4. Sequential stages of 3D-mesh deformations during the deployment of the AGF

### 3. COMPUTATIONAL STUDIES ON FLOW CONTROL ON ROTOR BLADES VIA ACTIVE GURNEY FLAP

Computational studies conducted in the program COMROTAG have been aiming at:

- validation of developed and implemented CFD codes against results of WTT,
- significant gain of knowledge about flow control through Active Gurney Flap in rotorcraft applications,
- conduction of computer simulations prior to flight tests of real rotor/helicopter (so called "blind tests"), in order to define the optimal scope of flight tests as well as to identify potentially dangerous phases of flight.

Computational studies have been conducted for both the 2D and 3D configurations.

#### 3.1. Two-Dimensional Studies on Flow Control on Rotor-Blade Segment via AGF

The subject of conducted two-dimensional experimental studies on AGF was the blade segment NACA0012 with thickened trailing edge and equipped with AGF. The angle of attack of the segment was fixed during every run, while the AGF was cyclically deployed and retracted. The same conditions were modelled in CFD simulations, including modelling of the three-dimensional space of the test-chamber inside. For these quasi-2D simulations, simplified version of the developed software (Virtual-Rotor-2.5D) intended to solve such problems has been used. Presented results refer to WTT conducted for flow velocity  $V=60\text{m/s}$ , 5Hz frequency of AGF oscillations and ramp schedule of AGF motion shown in Figure 5.

For the case of angle of attack  $\alpha=4\text{deg}$ , Figure 6 compares the CFD and WTT results in respect to time-variable lift ( $C_L$ ) and pitching moment ( $C_m$ ) coefficients measured during one period of AGF deployment-retraction cycle. While the time averaged computational and experimental values of  $C_L$  and  $C_m$  are similar, the computational result indicates strong oscillations, especially in the phase when the AGF is fully deployed. Such phenomenon is not observed in experimental results.

Presented in Figure 7 the frequency-domain analysis of time-varying pitching-moment coefficient ( $C_m$ ) shows, that for CFD results the dominant frequency of oscillations of global aerodynamic coefficients is approximately 545 Hz, which is close to 566 Hz - the dominant frequency of unsteady vortex shedding observed in other CFD results related to the static case with fully deployed AGF and  $\alpha=0\text{deg}$ . Figure 7 shows also dominant, but much weaker frequency 1100 Hz, which is close to 1123 Hz - the dominant frequency of unsteady vortex shedding observed in another CFD results concerning the static case with retracted AGF and  $\alpha=0\text{deg}$ . Unfortunately, the frequency-domain analysis of the experimental results does not indicate any dominant frequencies neither in proximity 592 Hz nor in proximity 1075 Hz, despite that these dominant frequencies were observed previously in WTT results in the static cases for both the AGF fully deployed and fully retracted ( $\alpha=0\text{deg}$ ). This is all the more surprising since the PIV results confirm the occurrence of unsteady vortex shedding in the discussed experimental case. One of possible explanation of this incoherence of WTT results is that the pressure-measuring signals were filtered, so the higher frequencies have been cut. Exemplary comparison of PIV results obtained in WTT and results of CFD simulation presented in terms of  $Q$ -criterion contours is presented in Figure 8.

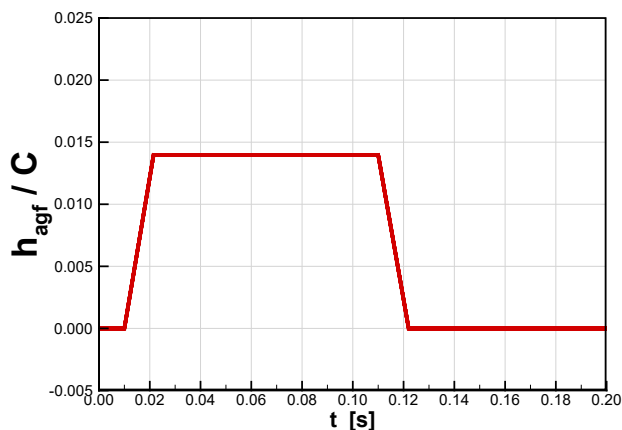


Fig. 5. Momentary height of the AGF ( $h_{agf}$ ) vs. time ( $t$ ) during one period of AGF deployment-retraction cycle

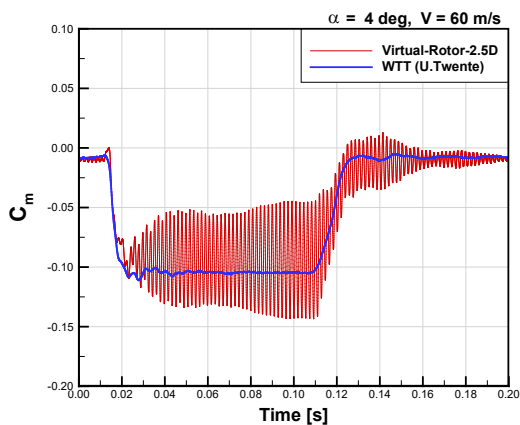
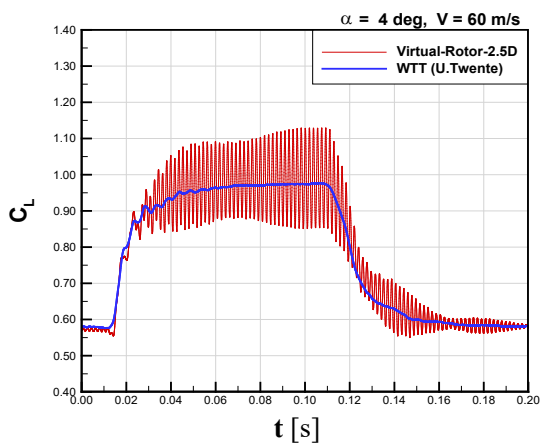


Fig. 6. Momentary lift coefficient ( $C_L$ ) and pitching moment coefficient ( $C_m$ ) vs. time ( $t$ ). Comparison of CFD and WTT results.  $\alpha=4\text{deg}$ ,  $V=60\text{m/s}$

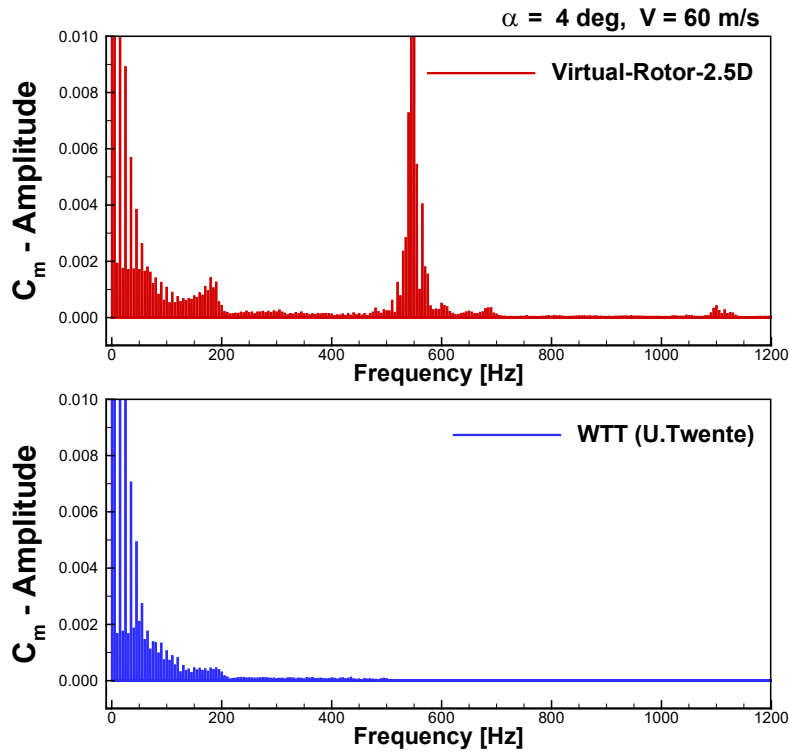


Fig. 7. Frequency-domain analysis of pitching moment coefficient  $C_m$ . Comparison of CFD and WTT results.  $\alpha=4\text{deg}$ ,  $V=60\text{m/s}$

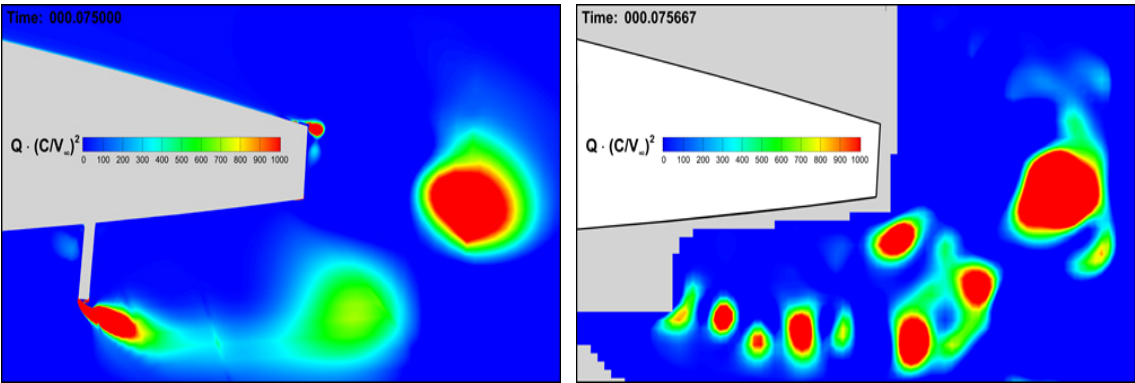


Fig. 8. Q-criterion contours at a moment of fully deployed AGF. Comparison of results of CFD (left picture) and WTT (right picture)

In Figure 9 the computational and experimental distributions of pressure coefficient ( $C_p$ ) on the airfoil surface are compared with each other for selected time moments corresponding to the AGF fully retracted and full deployed. The presented results show good convergence between the computational and experimental results.

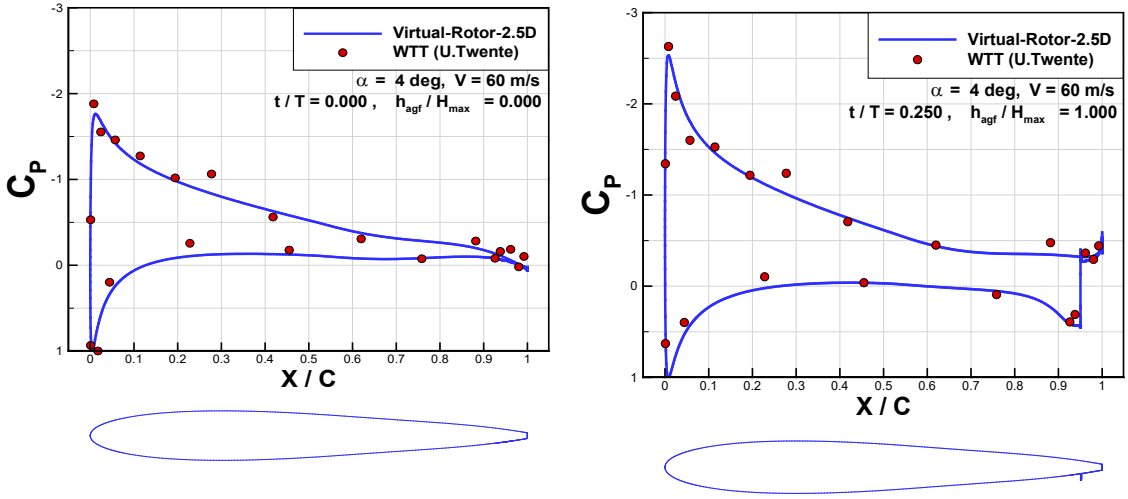


Fig. 9. Comparison of CFD and WTT results related to the pressure-coefficient ( $C_p$ ) distribution for AGF fully retracted (left) and fully deployed (right).  $\alpha=4\text{deg}$ ,  $V=60\text{m/s}$

The second discussed experimental case was run for angle of attack of  $12\text{ deg}$  and the schedule of the AGF motion similar to this utilised previously (see Figure 5). Figure 10 compares computational and experimental time-dependent lift ( $C_L$ ) and pitching moment ( $C_m$ ) coefficients measured during one period of AGF deployment-retraction cycle. The values of computational and experimental coefficient  $C_L$  and  $C_m$  are similar. Additionally, in the presented case, the CFD and WTT results indicate similar amplitudes and frequencies of oscillations of the coefficients  $C_L$  and  $C_m$ .

This similarity is confirmed when comparing the frequency-domain analyses of time-varying pitching moment coefficient ( $C_m$ ) presented in Figure 11. The graphs show lack of high dominating frequencies in both the CFD and WTT results. It is likely, that lack of strong vortex shedding of high frequencies, is a results of weak separation of flow on the upper surface of the blade segment, which may occur at angle of attack of  $12\text{ degree}$ . In a presence of flow separation, the vorticity flowing from the upper surface of the blade at its trailing edge is much weaker. This leads to weakening of the effect of counter rotating vortices flowing from upper and lower part of the blade trailing edge. Thus, the effect of high-frequency vortex shedding is significantly reduced in this case.

In Figure 12 the computational and experimental distributions of pressure coefficient ( $C_p$ ) on the airfoil surface are compared with each other for selected time moments corresponding to the AGF fully retracted and full deployed. These results confirm the hypothesis of flow separation on the upper surface of the airfoil, because they indicate characterising separated flows under-pressure at the trailing edge. Additionally, the presented results show very good convergence between the computational and experimental results.



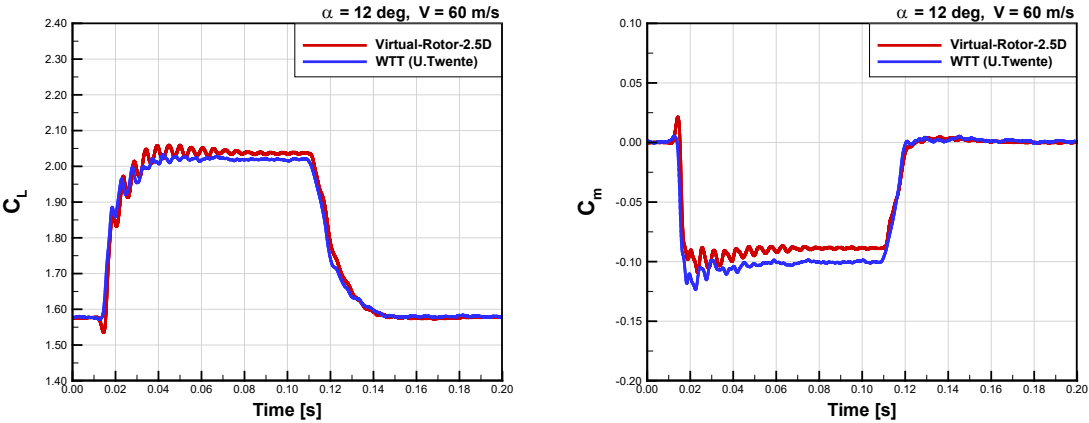


Fig. 10. Momentary lift coefficient ( $C_L$ ) and pitching moment coefficient ( $C_m$ ) vs. time (t). Comparison of CFD and WTT results.  $\alpha=12\text{deg}$ ,  $V=60\text{m/s}$

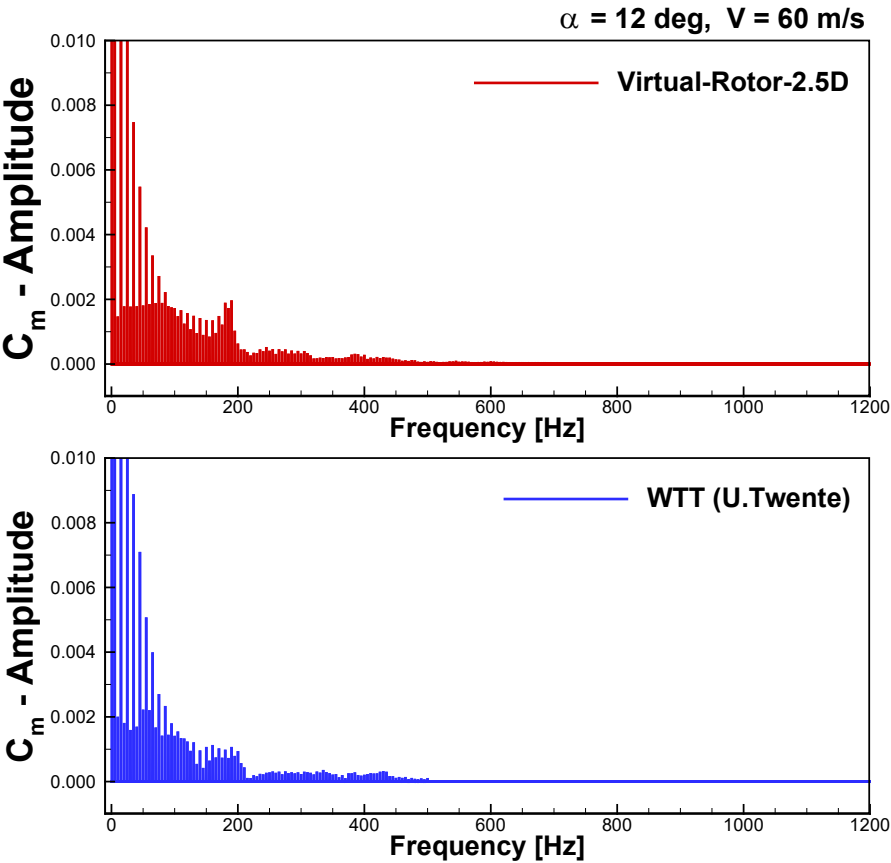


Fig. 11. Frequency-domain analysis of pitching moment coefficient  $C_m$ . Comparison of CFD and WTT results.  $\alpha=12\text{deg}$ ,  $V=60\text{m/s}$

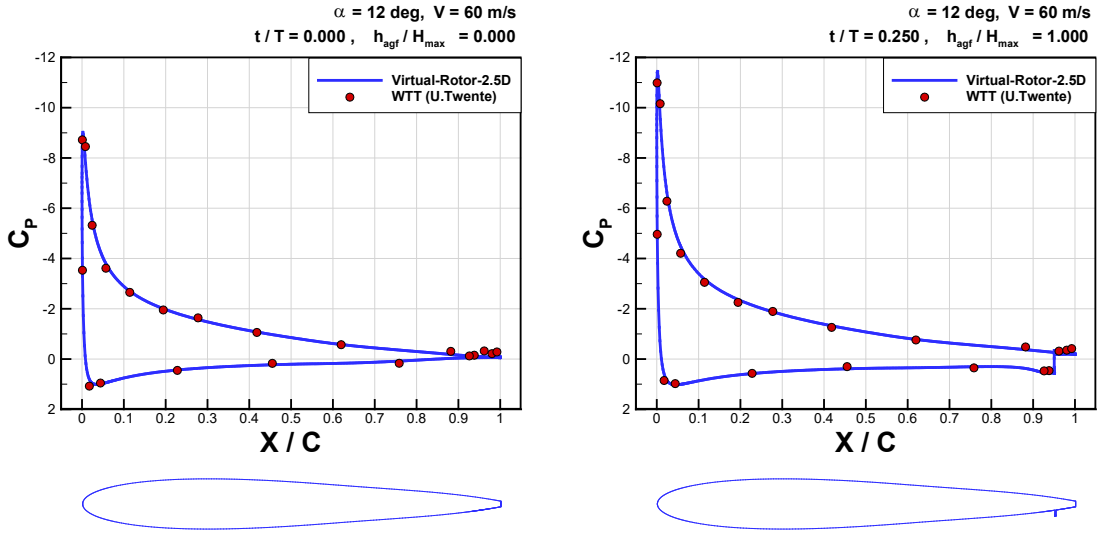


Fig. 12. Comparison of CFD and WTT results related to pressure-coefficient ( $C_p$ ) distribution for AGF fully retracted (left) and fully deployed (right).  $\alpha = 12^\circ$ ,  $V = 60$  m/s

Based on 2D version of the developed software a simplified sensitivity analysis has been conducted. The investigations were focused on searching for chordwise position and maximum height of the AGF, optimal from point of view of increase of lift force generated in a retreating-blade phase of airfoil motion.

The subject of conducted simulations was airfoil NACA0012 with thickened trailing edge. As shown in Figure 13, angle of attack ( $\alpha$ ) of the airfoil was changed harmonically with frequency 5Hz, within the range:  $1^\circ \div 10^\circ$ . Simultaneously the free-stream Mach number ( $M$ ) was changing within the range: from 0.15 for maximum angle of attack (retreating-blade-flow conditions) to 0.55 for minimum angle of attack (advancing-blade-flow conditions). The oscillating airfoil was equipped with the AGF deployed/retracted according to the sinusoidal schedule shown in Figure 13. In the conducted sensitivity analysis three chordwise positions of the AGF ( $X_{agf}$ ) at 96%, 98% and 100% of airfoil chord ( $C$ ) were considered as well as four maximum deployments of the AGF ( $H_{max}$ ): 0.5%, 1%, 1.5% and 2% of airfoil chord. The investigations aimed at determination of correlations between parameters  $X_{agf}$ ,  $H_{max}$  and the airfoil lift coefficient  $C_L$ .

Figure 14 presents time-variable lift coefficient captured during one period of oscillations, for the clean airfoil and for twelve different configurations of airfoil equipped with oscillating AGF. The oscillations of  $C_L$  visible in the presented graphs are probably the result of unsteady vortex shedding. Intensity and frequency of this phenomenon depends on parameters  $X_{agf}$ ,  $H_{max}$  as well as on the phase of the airfoil motion. Generally it may be concluded that intensity and frequency of unsteady vortex shedding tends to decrease within retreating-blade phase (the highest angles of attack) which results from possible flow separations (which was discussed in previous sub-section), the highest deployment of AGF, which gives the effect of „the thickest trailing edge” of the airfoil and from the lowest flow velocities occurring on the retreating blade.

As opposed to the results discussed in the first part of this sub-section, where the ramp schedule of AGF deployment was applied, in the currently discussed simulations expressly dominant frequencies

of unsteady vortex shedding have not been observed. This is the effect of continuous, harmonic changes of AGF height - one of the factors determining the unsteady vortex-shedding frequency. As the result, in the presented simulations, for the cases with active AGF, whole spectrum of frequencies of unsteady vortex shedding was observed. Visualisations of vortex shedding for selected AGF configurations are presented in Figure 15.

Figure 16 presents lift-growth coefficient  $\Delta C_{L(t)}$  as a function of AGF maximum height for three chordwise positions of the AGF. The coefficient  $\Delta C_{L(t)}$  expresses difference of momentary lift coefficients  $C_{L(t)}$  (defined based on momentary dynamic pressure) measured at moment corresponding to the retreating blade ( $t=0.10s$ ), for given AGF configuration and for the clean airfoil. Usually, the closer the AGF is placed to trailing edge, the smaller may be its maximum height. Therefore, the graph presented in Figure 16, should help to find optimal solution concerning the position and maximum height of designed AGF.

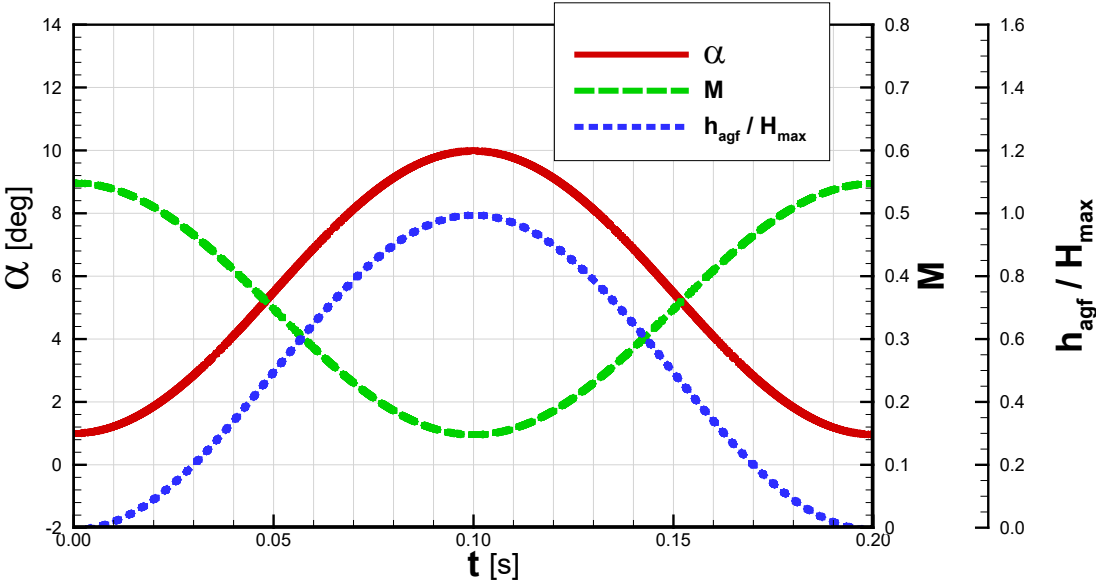
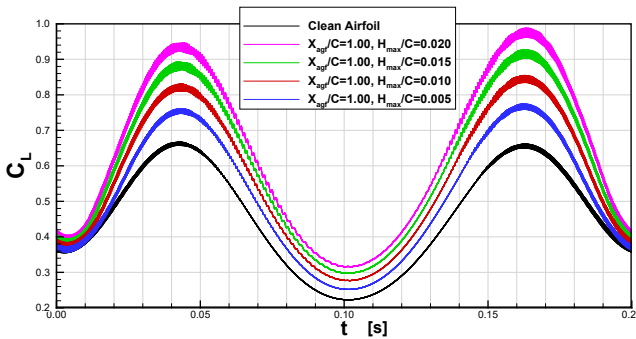


Fig. 13. Harmonic changes of angle of attack (a), free stream Mach number (M) and deployment of AGF ( $h_{agf}$ ) assumed in conducted 2D sensitivity analysis



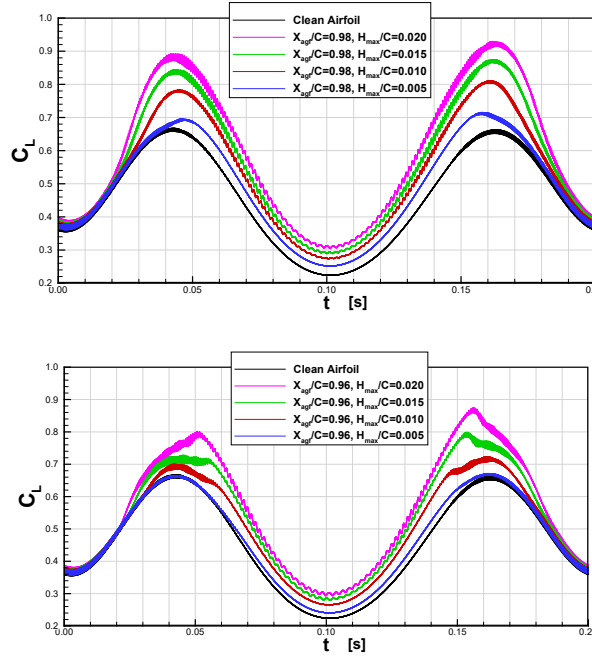


Fig. 14. Time-variable lift coefficient  $C_L$  captured during one period of oscillations, for the clean airfoil and for twelve configurations of airfoil equipped with oscillating AGF

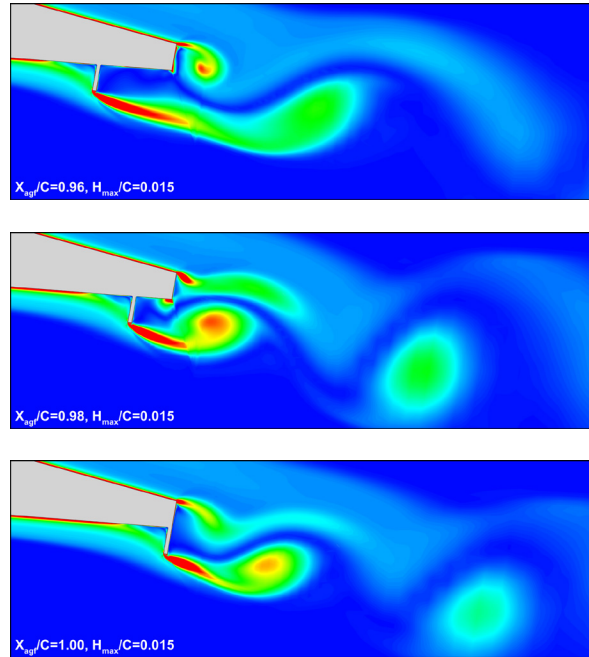


Fig. 15. Unsteady vortex shedding visualised through vorticity-magnitude contours, for maximum AGF deployment  $H_{max}/C=0.015$  and for three chordwise positions of the AGF

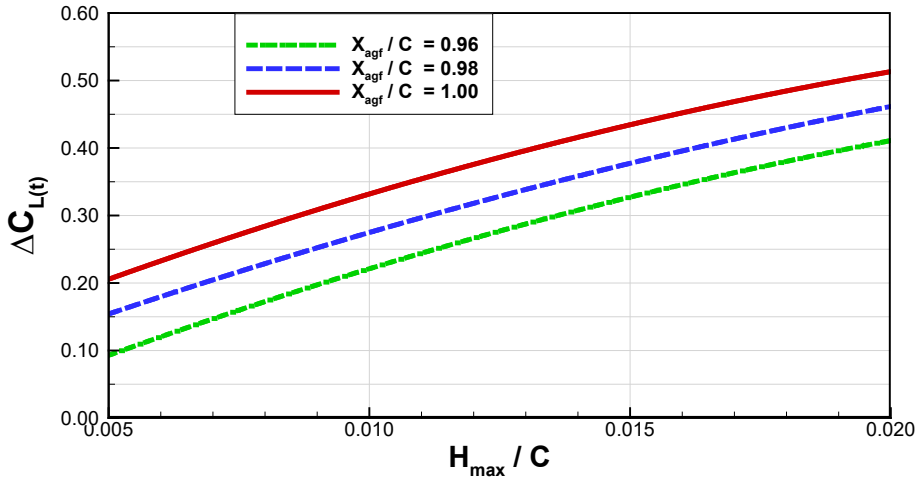


Fig. 16. Lift-growth coefficient ( $\Delta C_{L(t)}$ ) measured on retreating-blade, as a function of the AGF maximum height, for three chordwise positions of AGF

### 3.2. Three-Dimensional Studies on Flow Control on Rotor Blades via AGF

Three-dimensional, computational studies on flow control on rotor blades via AGF, have been conducted for the case of the 4-blade, fully articulated model rotor of radius 1.1m. Rotor rectangular blades of chord 0.09m were equipped with AGF in spanwise position from 53.5% to 68.5% of rotor radius. The maximum deployment of AGF was 2.78% of blade chord. The preliminary computational tests were conducted for two reference configurations: 1) rotor with Clean-Blades, 2) rotor with blades equipped with fixed, Passive Gurney Flap (PGF). The essential tests have been conducted for three configurations of AGF, differing in presented in Figure 17 schedules of AGF motion:

- 1) sinusoidal ( $h_{agf} = H_{max}$ :  $\Psi = 270\text{deg}$ ),
- 2) ramp-1 ( $h_{agf} = H_{max}$ :  $198\text{deg} \leq \Psi \leq 342\text{deg}$ ),
- 3) ramp-2 ( $h_{agf} = H_{max}$ :  $243\text{deg} \leq \Psi \leq 297\text{deg}$ ).

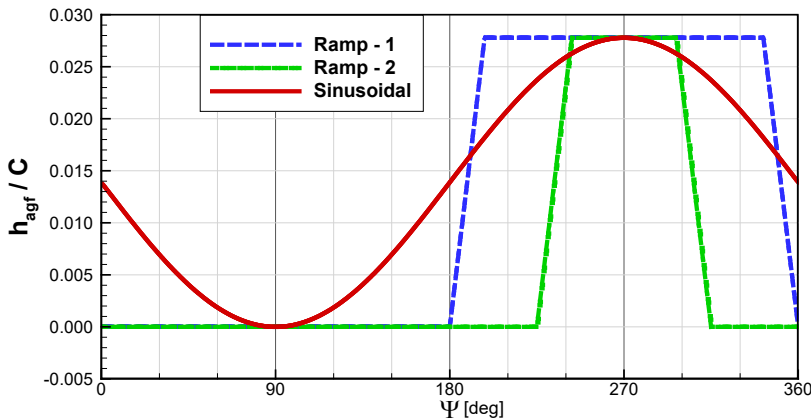


Fig. 17. Considered variants of AGF-motion schedules

Rotor forward-flight tests were conducted for flight conditions: velocity 48m/s, rotor rotational speed 1600 rpm, zero pitch and bank angles of the rotor shaft, atmosphere: Sea Level ISA. For each configuration the forward-flight simulations have been conducted for several commanded angles of collective pitch:  $\theta_0 = 4, 6, 8, 10$  and  $12$  deg. In each single simulation, the components of commanded cyclic pitch:  $\bar{\theta}=(\theta_s, \theta_c)$  were established so as to fulfil the “zero-flapping-trimming” requirements:

$$\bar{\beta}_1 = (\beta_{1s}, \beta_{1c}) = (0, 0) \quad 1)$$

where  $\beta_{1s}, \beta_{1c}$  are 1<sup>st</sup>-harmonic components of blade flapping. According to applied iterative trimming procedure, corrected cyclic pitch  $\bar{\theta}_n$  was evaluated according to the formula:

$$\bar{\theta}_n = \bar{\theta}_p - \left[ \frac{\partial \bar{\beta}_1}{\partial \bar{\theta}} \right]^{-1} \cdot \bar{\beta}_{1p} \quad 2)$$

where  $\bar{\theta}_p$  is the current cyclic pitch,  $\bar{\beta}_{1p}$  is the current vector  $\bar{\beta}_1$  and  $\left[ \frac{\partial \bar{\beta}_1}{\partial \bar{\theta}} \right]$  is a gradient matrix.

Selected results of CFD simulations conducted for two reference configurations: Clean-Blades and PGF, have been compared with analogous results of WTT [8]. Figure 18 compares CFD and WTT results concerning dependency of torque coefficient ( $C_{QUS}$ ) vs. thrust coefficient ( $C_{TUS}$ ) (referenced to rotor solidity  $\sigma$ ) for the Clean-Blades configuration. In this case the computational and experimental results agree with each other quite well. Differences are visible for the highest values of thrust coefficient where it is likely that significant retreating-blade stall occurs. Similar agreement of CFD and WTT results is visible in Figure 19, where computational and experimental dependencies: torque coefficient ( $C_{QUS}$ ) vs. thrust coefficient ( $C_{TUS}$ ) are compared for the Passive-Gurney-Flap configuration.

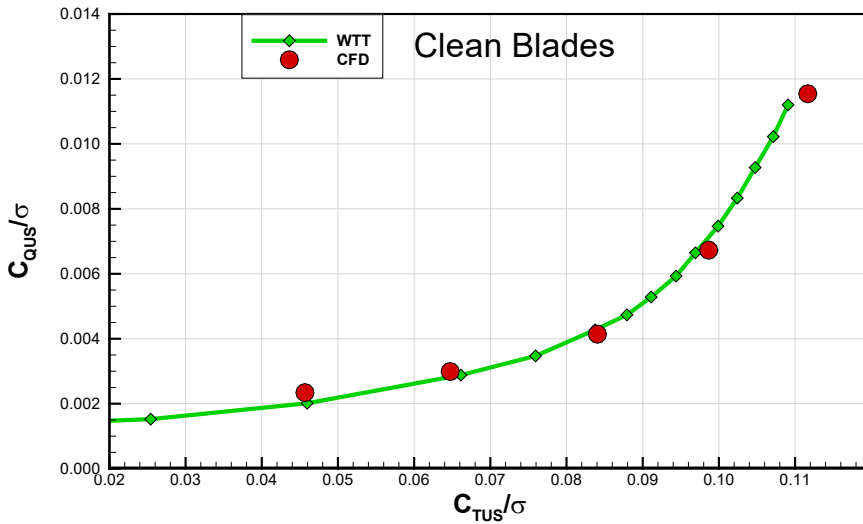


Fig. 18. Forward flight of Model Rotor at  $V=48\text{m/s}$ . Dependency ( $C_{QUS}/\sigma$ ) vs. ( $C_{TUS}/\sigma$ ). Results of CFD and WTT [8]. Clean-Blades configuration

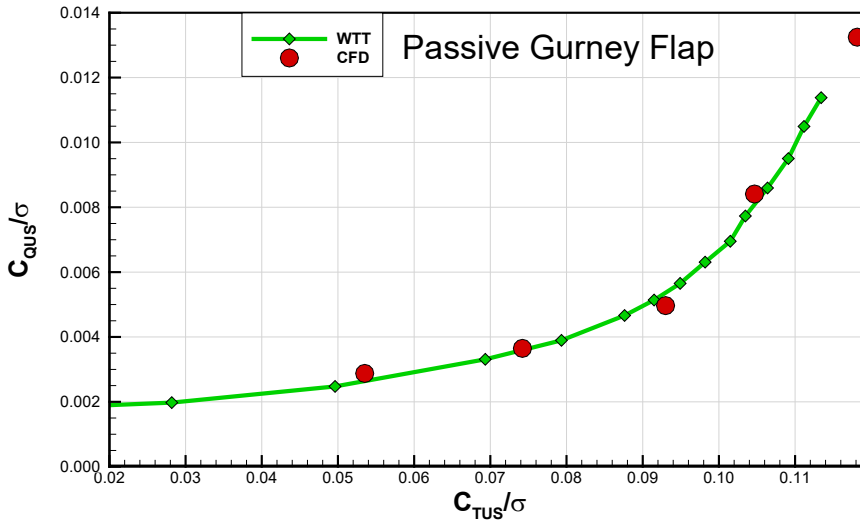


Fig. 19. Forward flight of Model Rotor at  $V=48\text{m/s}$ . Dependency ( $C_{QUS}/\sigma$ ) vs. ( $C_{TUS}/\sigma$ ). Results of CFD and WTT [8]. Passive-Gurney-Flap configuration

Figure 20 shows that application of PGF gives some performance benefits (i.e. generation of higher thrust for given torque) in comparison to Clean-Blades configuration but only above certain level of thrust coefficient (approx.  $C_{TUS}/\sigma > 0.084$ ). Analysing presented in Figure 20 results for the configuration AGF(sinusoidal), it may be concluded, that for higher values of thrust, this configuration gives similar performance benefits as PGF configuration. For lower values of thrust the AGF(sinusoidal) configuration does not indicate power penalty, observed for the PGF configuration. The above conclusions concern also the AGF(ramp-1) configuration which is shown in Figure 21. However, as shown in Figure 22, the AGF(ramp-2) configuration does not indicate any significant performance benefits.

Figure 23 presents relative (referenced to the Clean-Blade configuration) reduction of power (DP) necessary to drive the rotor, as a function of thrust coefficient referenced to a rotor solidity ( $C_{TUS}/\sigma$ ). This coefficient is presented for three configurations of rotor blades:

- Passive Gurney Flap,
- Active Gurney Flap of sinusoidal kinematics,
- Active Gurney Flap of ramp-1 kinematics

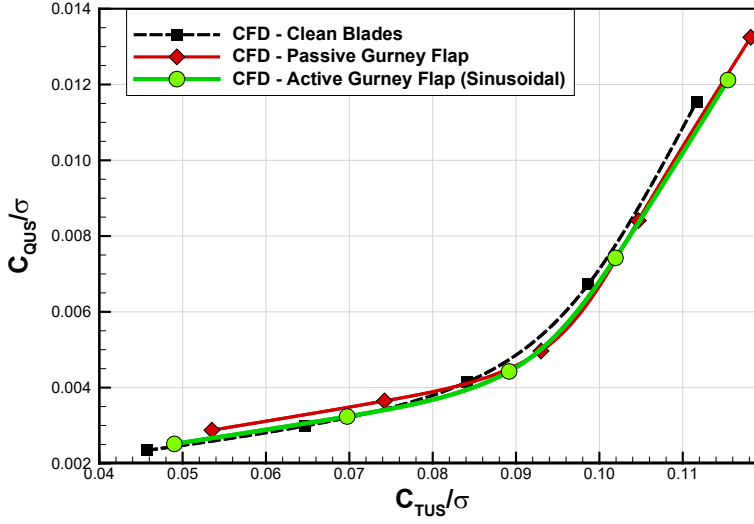


Fig. 20. Forward flight of Model Rotor at  $V=48\text{m/s}$ . Configurations: Clean-Blades, PGF and AGF (sinusoidal). Dependency ( $C_{QUS}/\sigma$ ) vs. ( $C_{TUS}/\sigma$ )

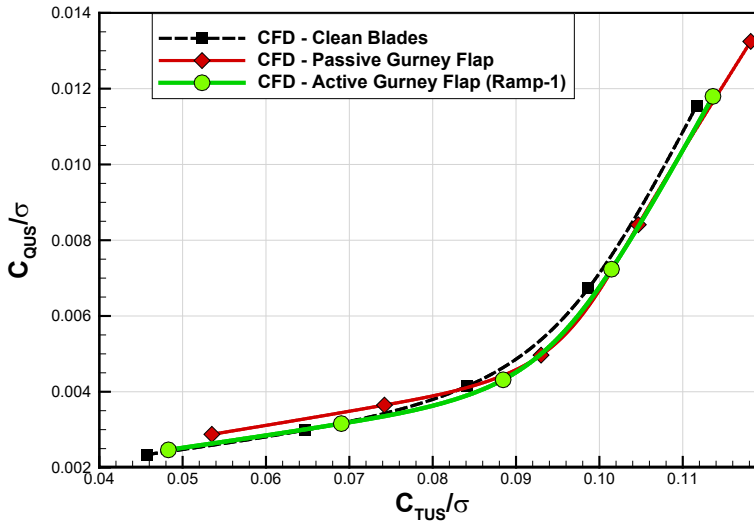


Fig. 21. Forward flight of Model Rotor at  $V=48\text{m/s}$ . Configurations: Clean-Blades, PGF and AGF (ramp-1). Dependency ( $C_{QUS}/\sigma$ ) vs. ( $C_{TUS}/\sigma$ )

The coefficient Power Reduction ( $\Delta P$ ) is defined as relative reduction of power ( $P$ ) with respect to the reference power ( $P_{(\text{clean blades})}$ ) corresponding to the Clean-Blade configuration:

$$\Delta P = (P_{(\text{clean blades})} - P) / P_{(\text{clean blades})} \quad 3)$$

$\Delta P$  positive means certain benefits in power reduction for given thrust.  $\Delta P$  negative mean unfavourable (negative) changes in power for the same value of thrust.



Based on the graphs presented in Figure 23, it may be concluded, that:

- For higher values of thrust coefficient, the configurations with Active Gurney Flap and Passive Gurney Flap indicate certain performance benefits in comparison to the Clean-Blades configuration.
- For lower values of thrust coefficient, the Passive-Gurney-Flap configuration indicates significant power penalty.
- Free of this disadvantage are Active-Gurney-Flap configurations, for which power penalty is relatively small.
- The AGF with Ramp-1 kinematics indicates slightly higher relative power reduction than AGF with Sinusoidal kinematics.

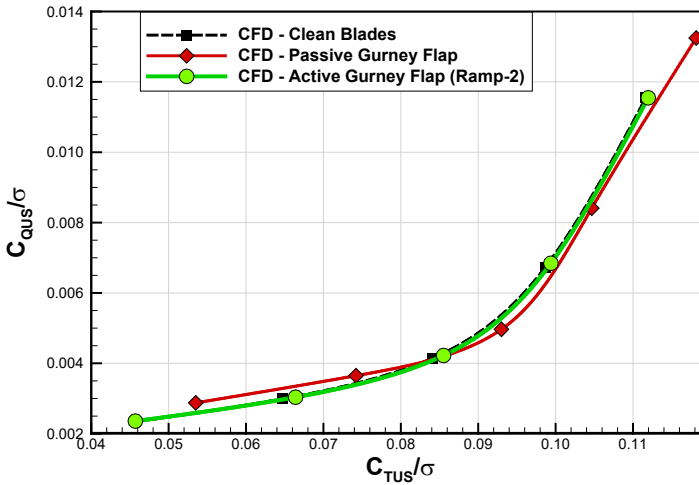


Fig. 22. Forward flight of Model Rotor at  $V=48\text{m/s}$ . Configurations: Clean-Blades, PGF and AGF(ramp-2). Dependency ( $C_{QUS}/\sigma$ ) vs. ( $C_{TUS}/\sigma$ )

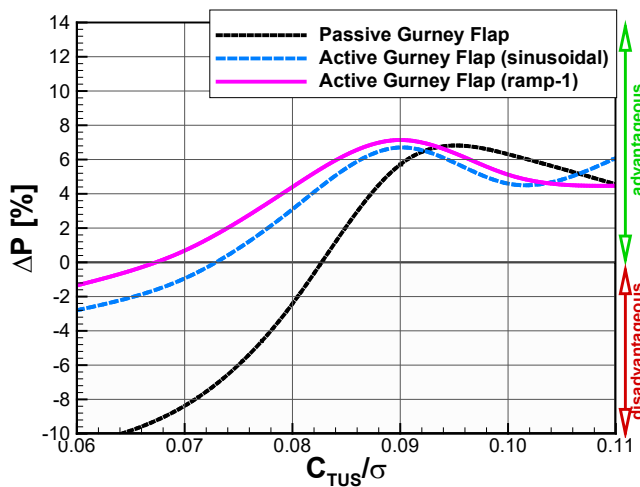


Fig. 23. Relative power reduction ( $\Delta P$ ) vs. thrust coefficient ( $C_{TUS}/\sigma$ ). Results obtained for the configurations: Passive Gurney Flap, Active Gurney Flap (sinusoidal) and Active Gurney Flap (ramp-1)

Figure 24 and Figure 25 compare vortex structures (visualised as Q-criterion iso-surfaces) generated by Clean-Blades and AGF(sinusoidal) configurations, for two collective-pitch angles  $\theta_0 = 6$  and 10 deg. As opposed to the case  $\theta_0 = 6$  deg, for the case  $\theta_0 = 10$  deg the strong retreating-blade stall is well visible for both compared configurations.

Moreover, the configurations with active AGF are characterised by significant vortex shedding from end-tips of deployed AGF, which is similar to formation of classic blade-tip vortices and which may be additional source of drag and noise (however, this unfavourable phenomenon in case of Active Gurney Flap is significantly reduced compared to Passive-Gurney-Flap configuration). In the case of Clean-Blades configuration, at the ends of the AGF zone, the local thickening of the trailing edge may also cause weak vortex shedding.

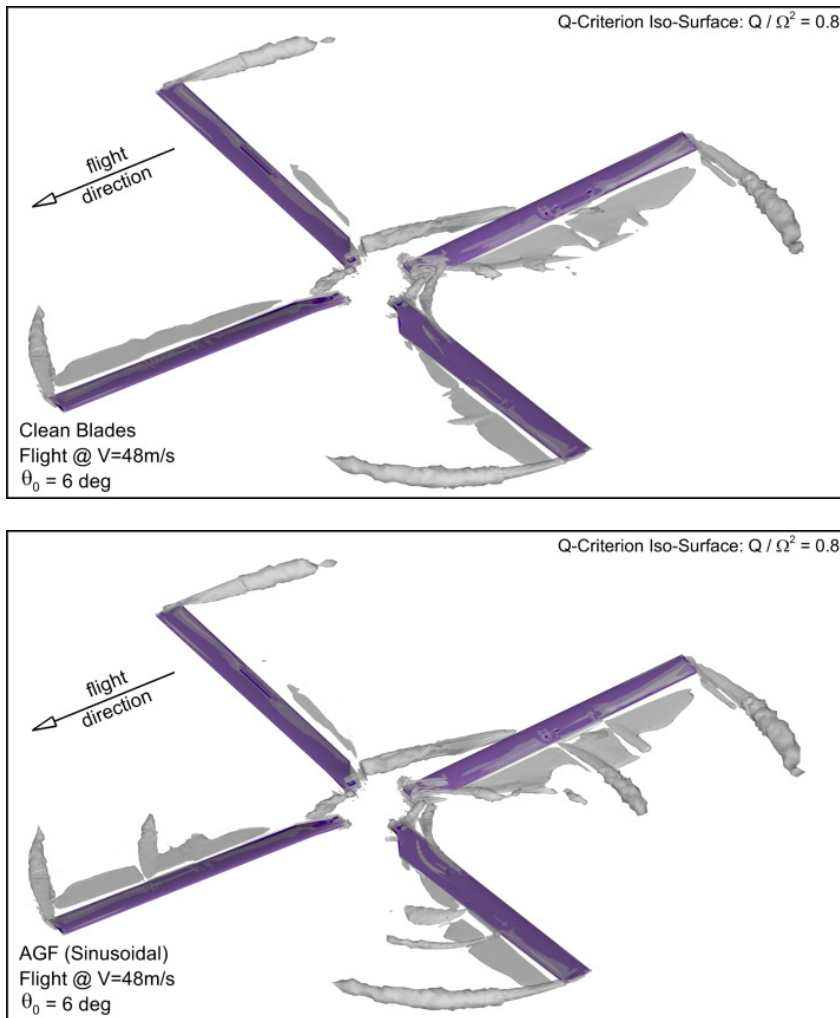


Fig. 24. Comparison of vortex structures for Clean-Blades and AGF(sinusoidal) configurations.  $\theta_0 = 6$  deg

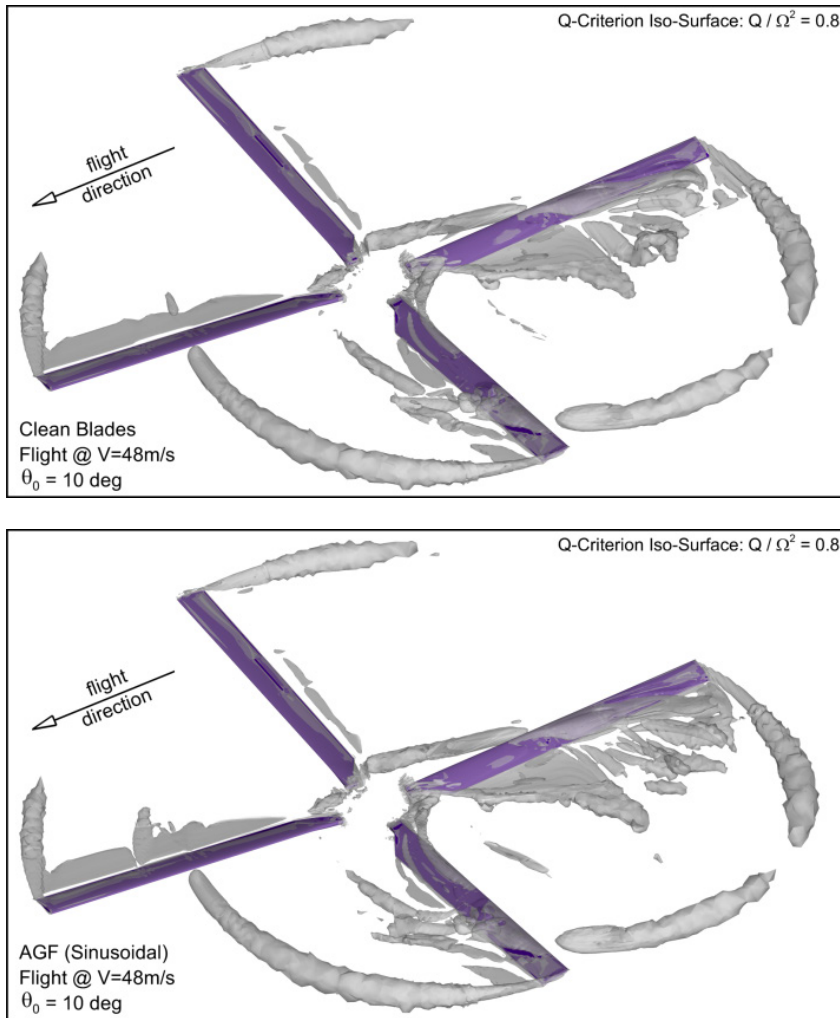


Fig. 25. Comparison of vortex structures for Clean-Blades and AGF (sinusoidal) configurations.  $\theta_0=10\text{deg}$

#### 4. SUMMARY AND CONCLUSIONS

The investigations discussed in the paper focused on phenomena occurring in the flow around helicopter-rotor blades equipped with Active Gurney Flaps (AGF). Validation of the developed CFD codes confirmed good agreement of computational and experimental results, concerning both the quasi-2D and 3D test cases. Conducted simplified sensitivity analysis has aimed at determination of geometric and motion-control parameters of the AGF, optimal from point of view of helicopter-performance improvement.

Truly 3D studies on investigated phenomena have been conducted for the case of forward flight of model rotor, considering:

- two reference configurations: Clean-Blades and Passive Gurney Flap (PGF),
- three configurations with Active Gurney Flaps, differing in schedules of AGF motion: „sinusoidal”, „ramp-1” and „ramp-2”

Performance benefits have been evaluated based on analysis of dependency: torque vs. thrust, favouring these configurations, which for given torque have generated the highest thrust. Based on obtained computational results, it may be concluded that:

- For higher values of thrust (likely in presence of retreating-blade stall), the configurations with active AGF give certain performance benefits in comparison to the Clean-Blades configuration, similar to the benefits of the PGF configuration.
- For lower values of thrust, the configurations with AGF, do not indicate the strong power penalty, observed for the PGF configuration.
- Above advantages of the AGF concern configurations of both the „sinusoidal” and „ramp-1” schedules of motion, but they do not concern the schedule „ramp-2” (characterised by a shortened phase of full deployment of AGF) which has not indicated any performance benefits.
- Compared to the Clean-Blades configuration, the AGF and PGF configurations are characterised by significant vortex shedding from end-tips of deployed Gurney Flap.

## NOMENCLATURE

C	blade chord	V	velocity
$C_L$	lift coefficient	$X_{agf}$	chordwise position of the AGF
$C_{L(t)}$	lift coefficient based on moment. dyn. pressure	$\alpha$	angle of attack
$\Delta C_{L(t)}$	coefficient of growth of $C_{L(t)}$	$\beta_{1S}, \beta_{1C}$	1 <sup>st</sup> -harmonic components of blade flapping
$C_p$	pressure coefficient	$\theta_0$	commanded collective pitch
$C_{QUS}$	torque coefficient (US convention)	$\theta_S, \theta_C$	components of commanded cyclic pitch
$C_{TUS}$	thrust coefficient (US convention)	$\sigma$	rotor solidity
$h_{agf}$	momentary height of AGF	$\Psi$	blade azimuthal position
$H_{max}$	maximum height of AGF		
M	Mach number	AGF	Active Gurney Flap
P	power	CFD	Computational Fluid Dynamic
$\Delta P$	relative reduction of power	PGF	Passive Gurney Flap
Q	Q-criterion factor	PIV	Particle Image Velocimetry
t	time	WTT	Wind Tunnel Tests

## BIBLIOGRAPHY

- [1] Gardner A.D., Richter K., Rosemann H., Numerical Investigation of Air Jets for Dynamic Stall Control on the OA209 Airfoil, Proceedings of ERF 2010, Paris, 7-9 September 2010.
- [2] Heine, B., Mulleners, K., Gardner, A., Mai, H., On the effects of leading edge vortex generators on an OA209 airfoil, ODAS2009, 2009.
- [3] Feszty D., Gillies E.A., Vezza M., “Alleviation of Airfoil Dynamic Stall Moments via Trailing-Edge Flap Flow Control”, AIAA Journal, Vol. 42, No. 1 (2004), pp. 17-25.
- [4] Wang, J.J., Li Y.C., Choi K-S., Gurney flap – Life enhancement, mechanisms and applications, Progress in Aerospace Sciences 44 (2008), pp. 22-47.
- [5] Active Gurney Flap, European Patent Application No. 11250481.6, Applicant: Claverham Limited Bristol.
- [6] ANSYS, Inc., ANSYS FLUENT User’s Guide. Release 15.0, November 2013. Available from: <http://www.ansys.com>.

- [7] Kinzel M.P., Maughmer M.D., Duque E.P.N, Numerical Investigation on the Aerodynamics of Oscillating Airfoils with Deployable Gurney Flaps, AIAA Journal Vol.48, No.7, July 2010.
- [8] Gibertini G., Zanotti A., New Technique Implementation in GVPM, Deliverable Report of Clean-Sky Project GUM, GUM/WP2/D2.3, July 2015.

---

## STEROWANIE PRZEPŁYWEM NA ŁOPATACH WIRNIKA NOŚNEGO ŚMIGŁOWCA

### Streszczenie

Aktywna Klapka Gurneya to niewielka, płaska płytką cyklicznie wysuwana i chowana prostopadle do dolnej powierzchni łopaty wirnika śmigłowca, ulokowana zazwyczaj w pobliżu krawędzi spływu łopaty. Zakłada się, że urządzenie może poprawić osiągi nowoczesnych helikopterów. Głównym celem prezentowanych badań było opracowanie odpowiedniej metodologii, a następnie użycie jej w badaniach zjawisk aerodynamicznych zachodzących w opływie łopat wirnika śmigłowca, wyposażonych w poruszające się klapki Gurneya. Przeprowadzone symulacje przepływu miały na celu walidację opracowanej metodyki, a także znaczne jej ulepszenie i rozbudowę, m.in. w oparciu o dostępne wyniki badań eksperymentalnych. Analiza wrażliwości została przeprowadzona w oparciu o uproszczoną 2/2,5-wymiarową analizę przepływu i miała ona na celu określenia parametrów geometrycznych i sterowania, optymalnych z punktu widzenia poprawy osiągnięć śmigłowca. W pełni trójwymiarowe symulacje lotu wirnika miały na celu określenie stanów lotu śmigłowca, w których zastosowanie Aktywnych Kłapek Gurneya mogłoby istotnie polepszyć osiągi wiroplata.

Słowa kluczowe: łopaty wirnika śmigłowca, aktywne sterowanie przepływem, Aktywna Klapka Gurneya, osiągi wiroplatów.

### Acknowledgements

The research leading to these results was financed by the European Union's Seventh Framework Programme (FP7/2007-2013) for the Clean Sky Joint Technology Initiative under grant agreement No.CSJ-GA-2013-619627 and by the Ministry of Science of Poland from funds directed to supporting scientific research, under agreement No.3129/CLEANSKY/2014/2.

Computational support was obtained from University of Warsaw Interdisciplinary Centre for Mathematical and Computational Modelling, in the Computational Grant No.G52-4.